Supporting Information

Virus inhibition induced by polyvalent nanoparticles of different sizes

Jonathan Vonnemann, Christian Sieben, Christopher Wolff, Kai Ludwig, Christoph Böttcher*, Andreas Herrmann*, and Rainer Haag*

Table of Contents

Confirmation of quantitative sulfation of TA-PGOH-[G1]

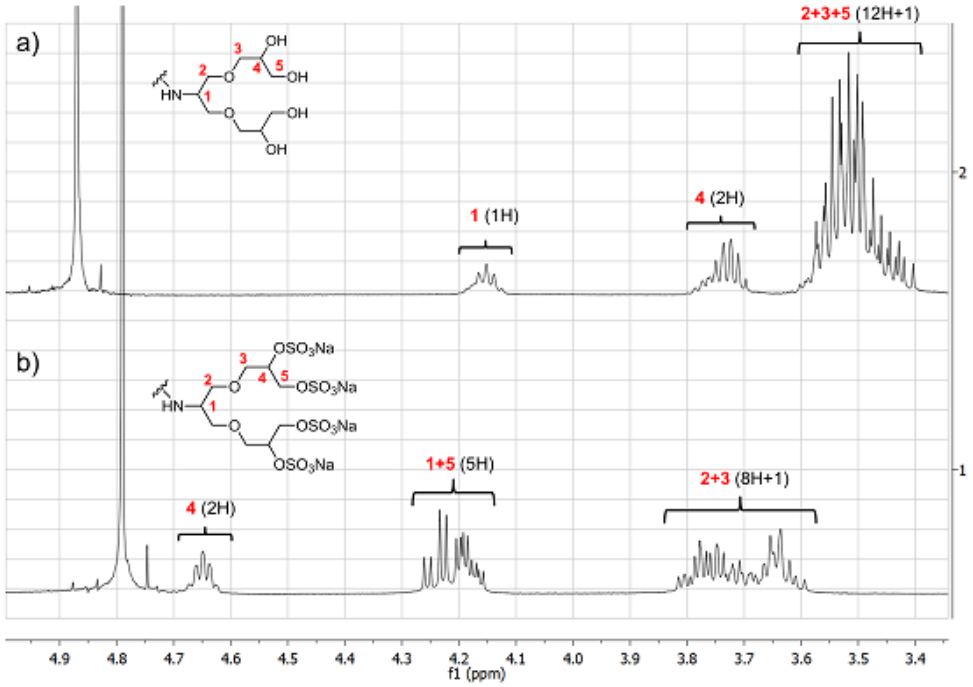

Fig. S1 ^{1}H-NMR of the PG-backbone for (a) TA-PGOH-[G1] dendron in CD_3OD and (b) TA-PGS-[G1] dendron in D_2O. The integrals of the downfield shifted protons in α-position to the sulfate moieties verify a quantitative conversion. The extra proton occurring in the range of 3.5-3.9 ppm is therefore based on the methylene group in α-position to the disulfide group of the thioctic acid moiety.

NMR Spectra

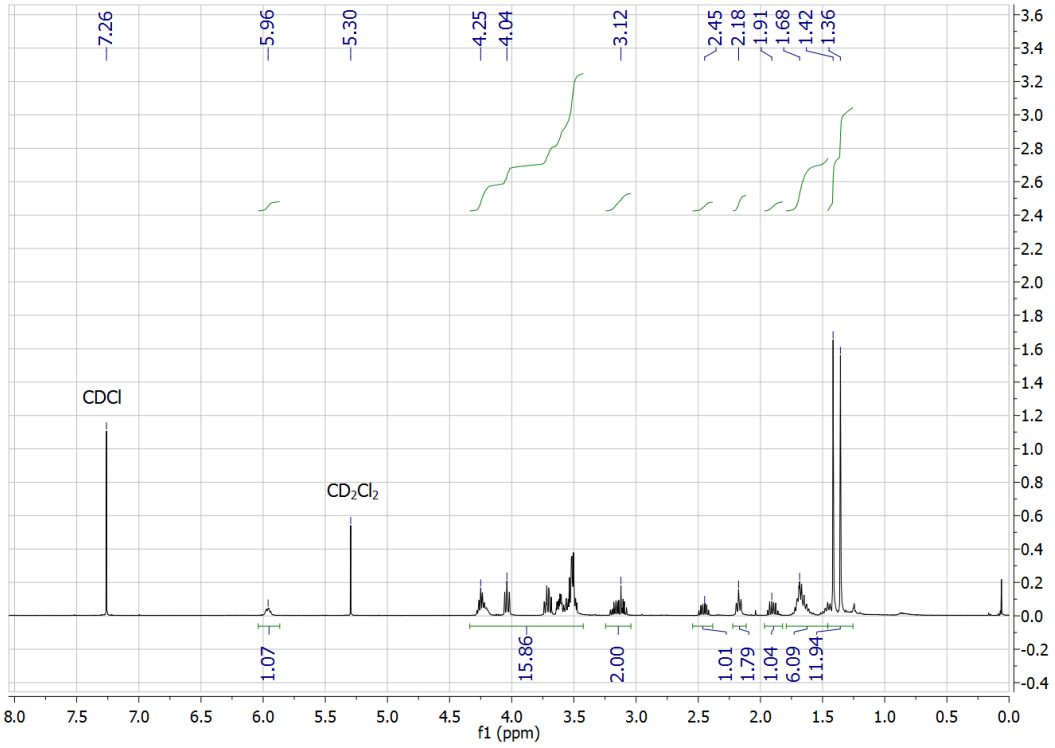

Fig. S2 TA-PG-acetal-[G1] dendron (^{1}H-NMR, 400 MHz, $CDCl_3$).

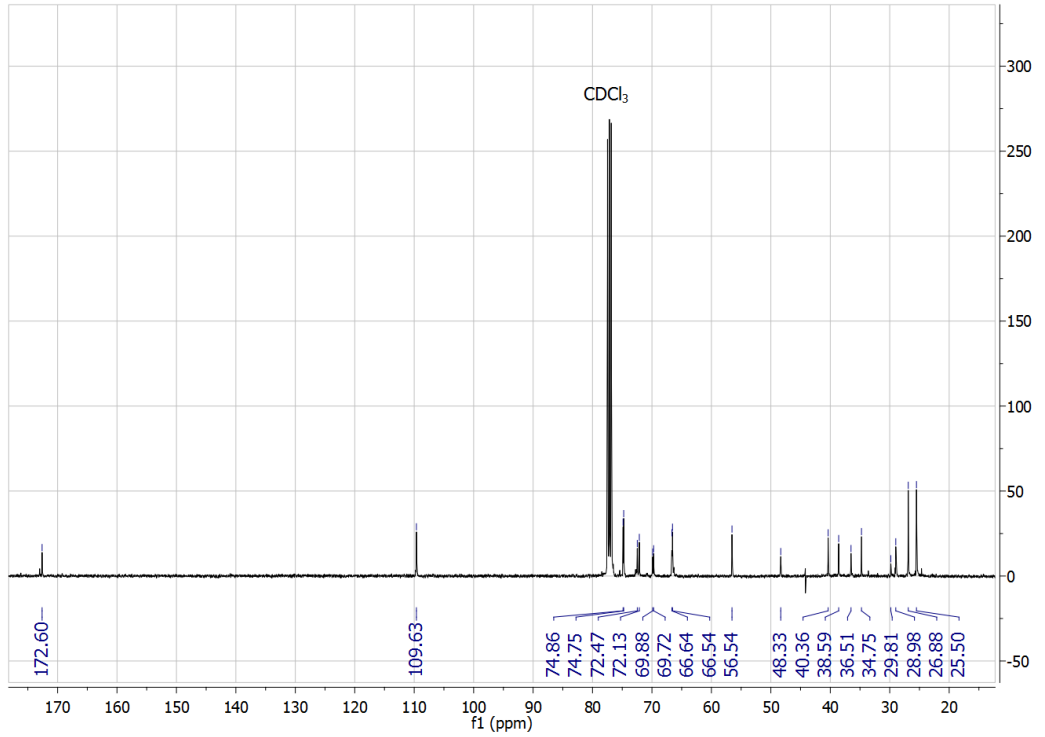

Fig. S3 TA-PG-acetal-[G1] dendron (^{13}C-NMR, 400 MHz, $CDCl_3$).

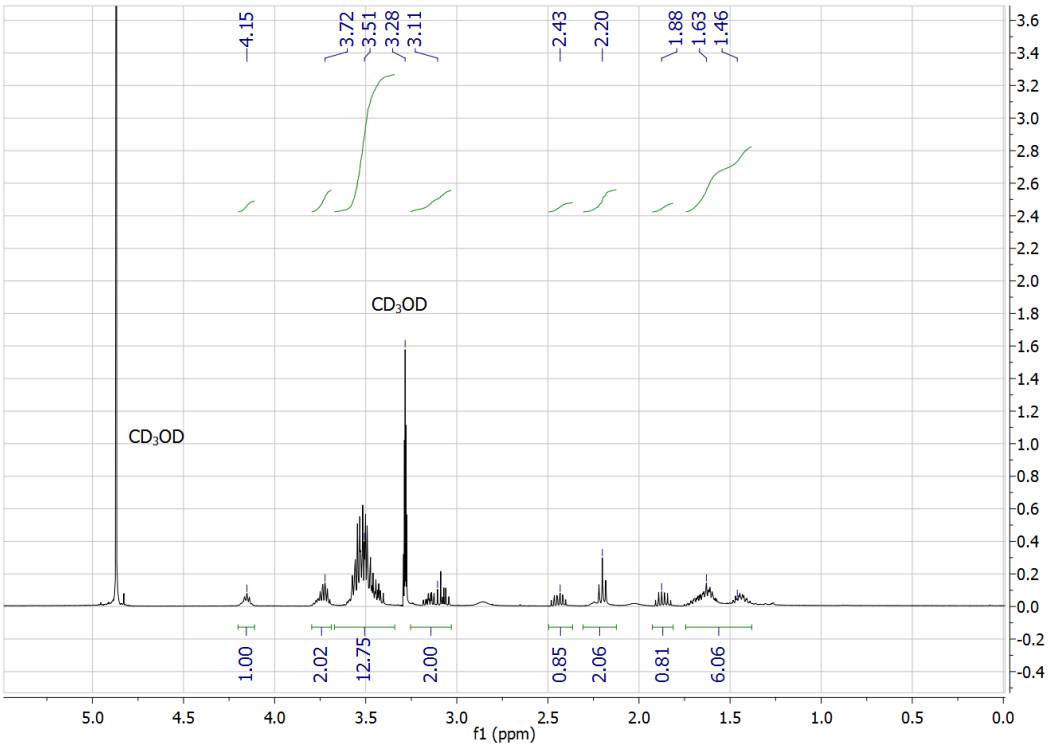

Fig. S4 TA-PGOH-[G1] dendron (^{1}H-NMR, 400 MHz, CD_3OD).

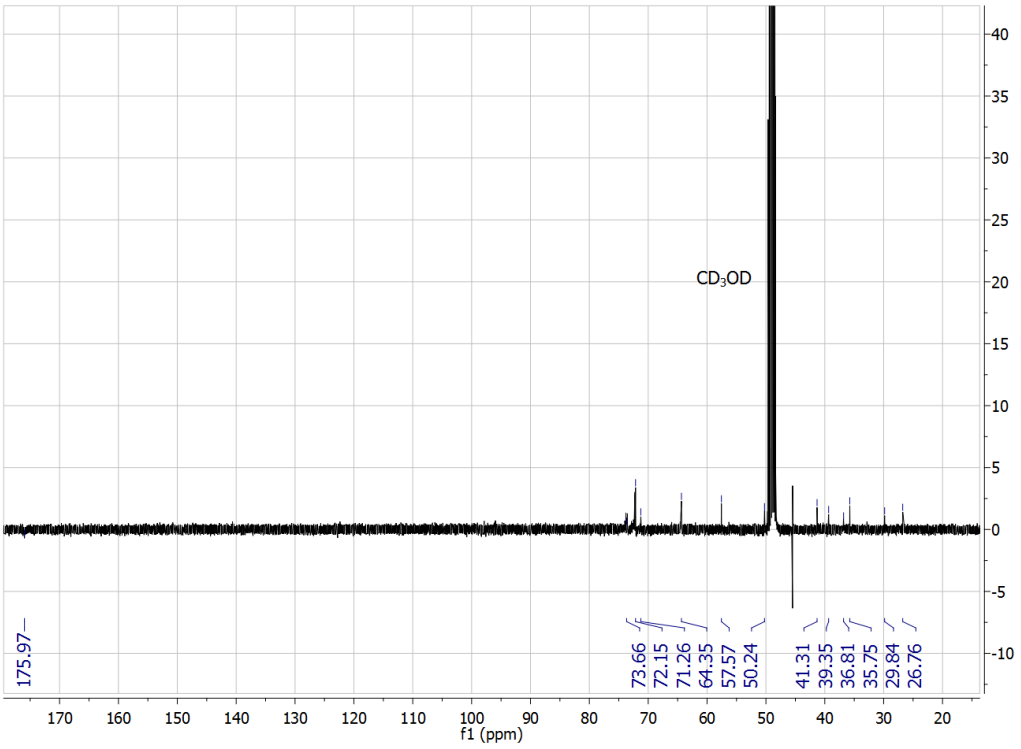

Fig. S5 TA-PGOH-[G1] dendron (^{13}C-NMR, 400 MHz, CD_3OD).

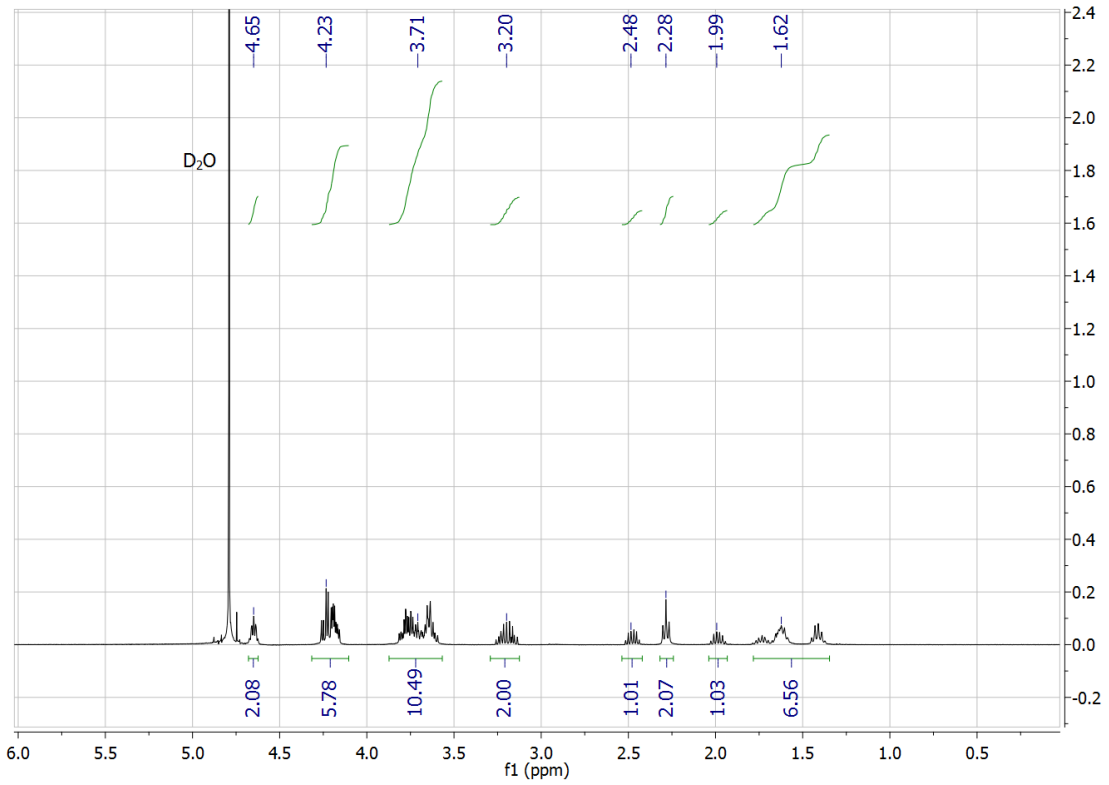

Fig. S6 TA-PGS-[G1] dendron (^{1}H-NMR, 400 MHz, D_2O).

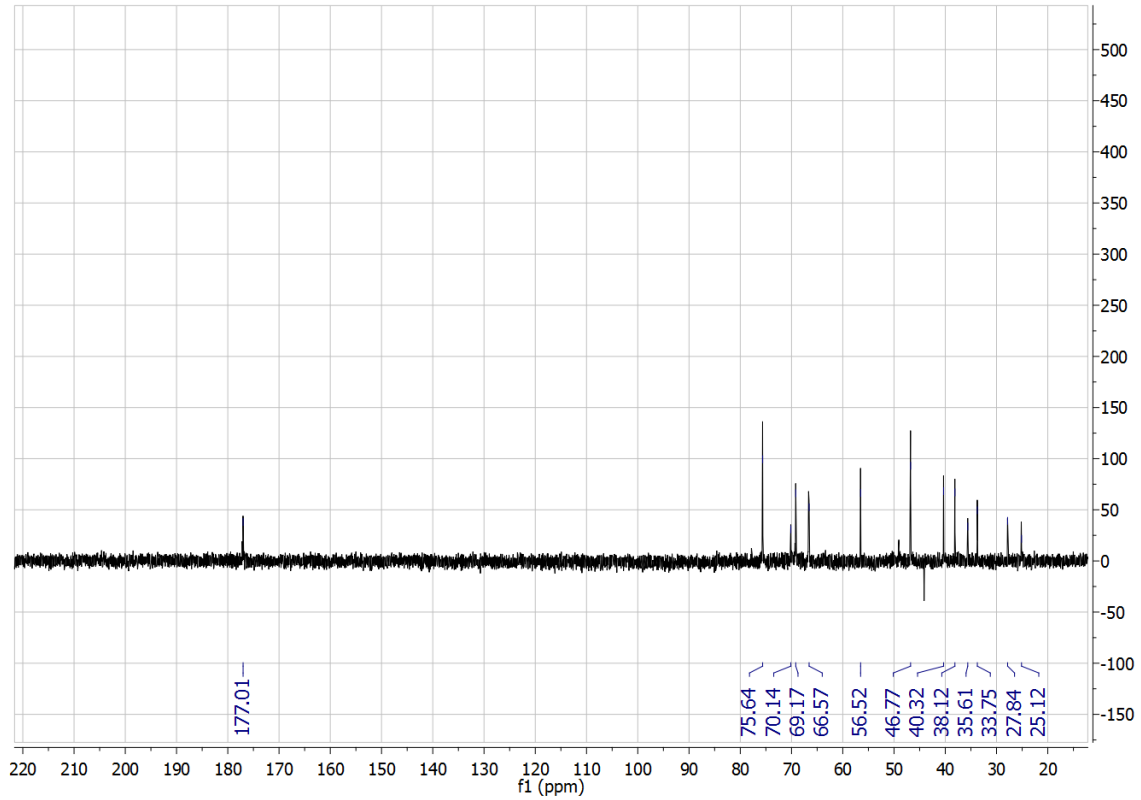

Fig. S7 TA-PGS-[G1] dendron (^{13}C-NMR, 400 MHz, D_2O).

Determination of the required ligand amount for a quantitative particle functionalization

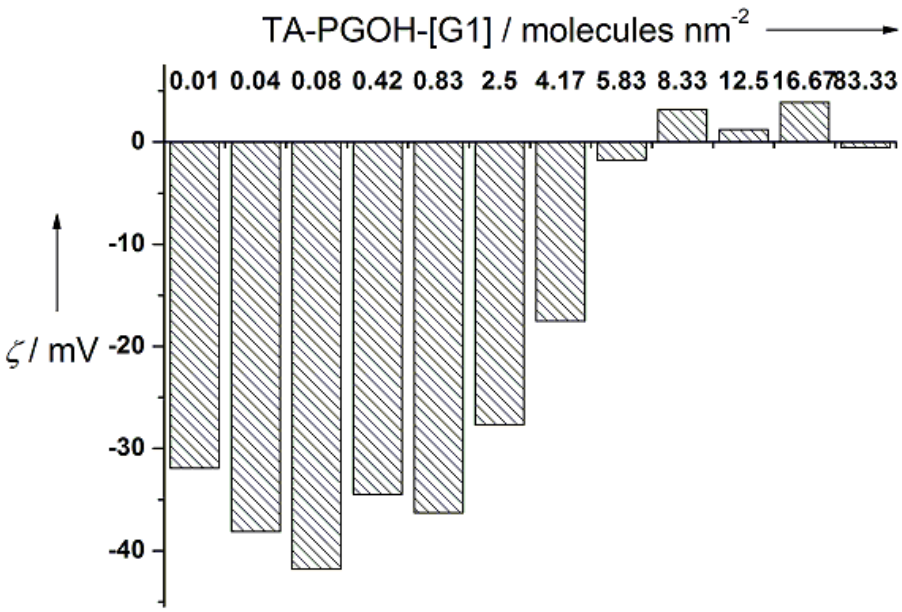

Fig. S8 Zeta-potential of 19 nm AuNP-OH at increasing ligand density. At six or more ligands per nm^2 a complete replacement of the citrate by TA-PGOH-[G1] dendron was observed.

TEM and DLS measurements of synthesized gold nanoparticles

a)

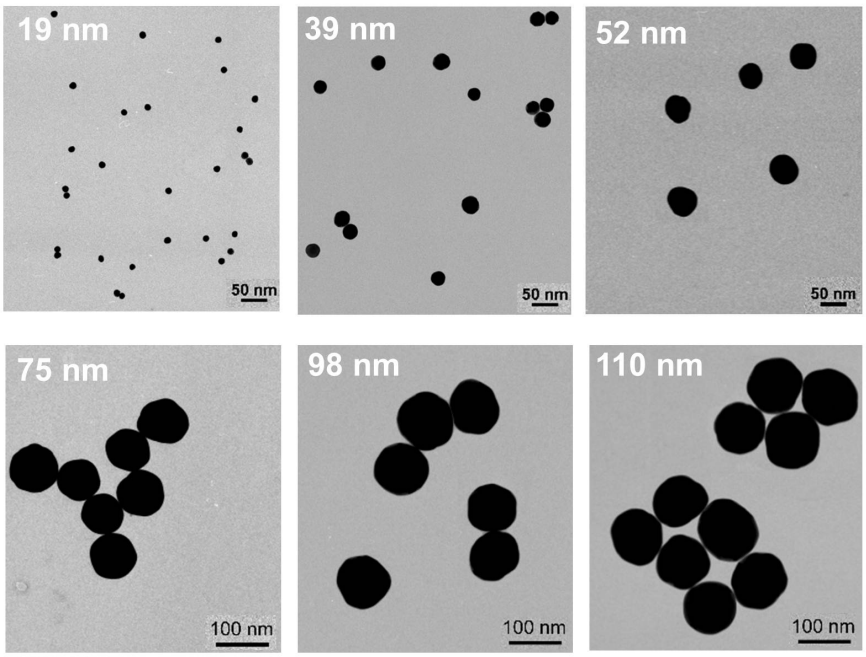

b)

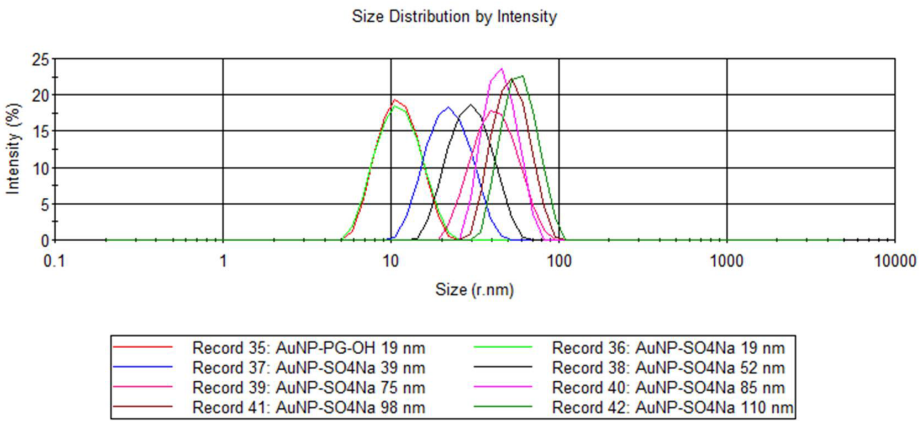

Fig. S9 (a) TEM micrographs of the synthesized AuNP-SO_4Na at different sizes. (b) DLS measurements: Size distribution by intensity of the synthesized AuNP-SO_4Na.

Table S1 Z-Average diameter of synthesized nanoparticles with the respective PDIs according to DLS measurements.

$Diameter_{AuNP\text{-}Citrate}$ [nm]	$Diameter_{AuNP\text{-}Sulfate}$ [nm]	$PDI_{AuNP\text{-}Citrate}$ [a.u.]	$PDI_{AuNP\text{-}Sulfate}$ [a.u.]
17.41	20.96	0.044	0.078
39.12	41.61	0.074	0.078
52.11	56.5	0.076	0.07
75.38	87.92	0.075	0.083
85.84	87.61	0.009	0.014
98.03	101.5	0.033	0.028
110	114.2	0.011	0.02

Determination of AuNP-SO_4Na concentration

Atomic Absorption Spectroscopy (AAS) measurements were conducted for the determination of the gold concentration (C_{Au}) within the colloidal solutions. For a standard AAS experiment, 1 ml of the colloidal solution was dissolved in 2 ml *aqua regia* for 30 min. After the addition of water (12 ml), the reaction mixture was agitated and used for AAS measurements. The resulting C_{Au} was subsequently multiplied with a factor of 15 due to the previous dilution. Assuming a perfect spherical form for the gold nanoparticles, the molar mass (M), the molar surface area (A), the concentration of gold nanoparticle (C) and the gold nanoparticle area concentration (AC) for each particle size was calculated via Equation S1, S2, S3 and S4. The required diameter of the gold nanoparticles for the calculation of the nanoparticle volume was hereby taken from statistical analysis of the transmission electron micrographs, while the diameter for the area calculation was obtained from the dynamic light scattering results of the ligand-functionalized nanoparticles. The diameter of the gold nanoparticles (d_{AuNP}) used in following equations were given in nm.

$$M_{AuNP} = \frac{\pi \cdot (d_{AuNP} \cdot 10^{-7})^3 \cdot N_A \cdot \delta_{Au}}{6} \left[\frac{g}{mol}\right] \quad \text{(eq.S1)}$$

$$A_{AuNP} = \pi \cdot (d_{AuNP} \cdot 10^{-9})^2 \cdot N_A \left[\frac{m^2}{mol}\right] \quad \text{(eq.S2)}$$

$$C_{AuNP} = \frac{C_{Au}}{M_{AuNP}} \left[\frac{mol}{l}\right] \quad \text{(eq.S3)}$$

$$AC_{AuNP} = C_{AuNP} \cdot A_{AuNP} \left[\frac{m^2}{l}\right] \quad \text{(eq.S4)}$$

The results are presented in Table S2.

Table S2: Molar mass and molar surface area of synthesized gold nanoparticles

$Diameter_{AuNP}$ [nm]	M_{AuNP}[g/mol]	A_{AuNP}[m^2/mol]
19.41	4.45E+07	7.13E+08
39.12	3.65E+08	2.90E+09
52.11	8.62E+08	5.14E+09
75.38	2.61E+09	1.07E+10
85.84	3.85E+09	1.39E+10
98.03	5.74E+09	1.82E+10
110	8.11E+09	2.29E+10

By calculating the concentration of each colloidal stock solution according to Equation S3, the molar extinction coefficient at $\lambda_{450\ nm}$ was determined via the slope of concentration dependent UV-Vis calibration curves. The resulting extinction coefficients were compared with calculated extinction coefficients from the Mie-theory and confirmed an accurate concentration determination for all particle size.[1] The comparison of the experimental and theoretical extinction coefficients is depicted in Figure S10.

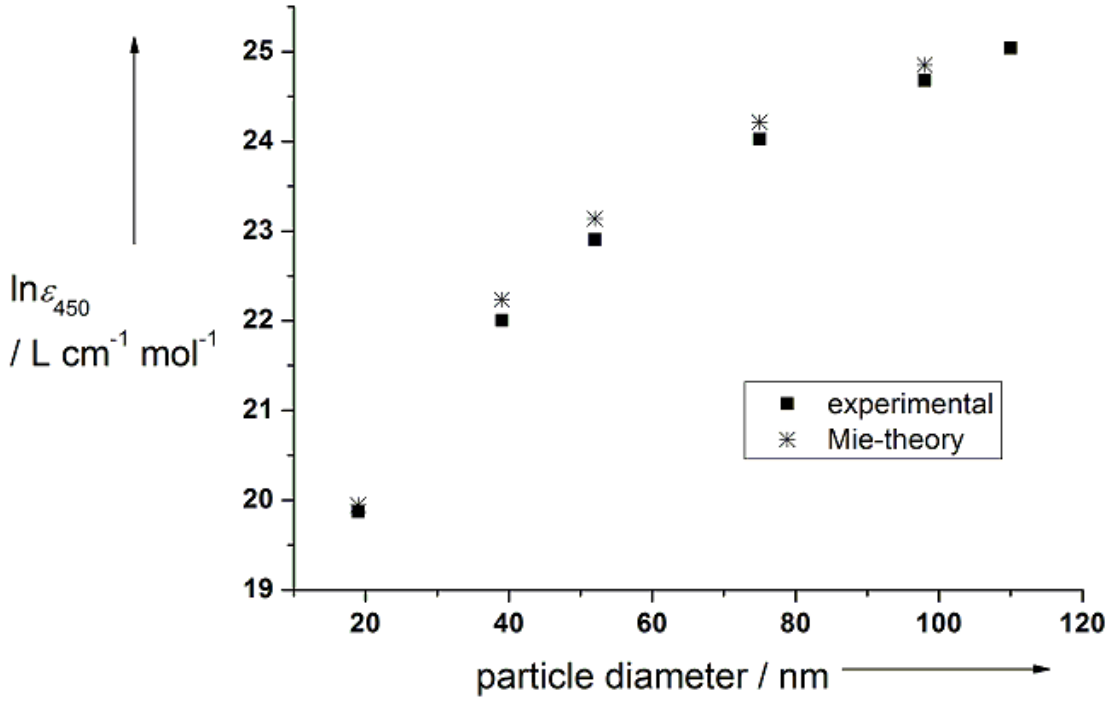

Fig. S10 Comparison of experimentally determined extinction coefficients at $\lambda_{450\ nm}$ and theoretically calculated extinction coefficients via Mie Theory.[1]

Investigation of the viral binding function

Pure VSV preparations at pH 7.5 show by TEM that virions do not spontaneously aggregate and are evenly distributed over the grid. Almost all virions are bullet-shaped and present an intact G protein layer. These observations are in agreement with those reported by Libersou et al.[2] However, as a consequence of the lacking proofreading ability of the viral RNA polymerase and the resulting known high mutation rate of VSV, defects can render the virions non-infectious but still physically intact.[3,4] Considering a significant number of non-infectious particles, we assume that some of the mutations may interfere with the function of the viral G protein and influence virus binding efficiency accounting for unbound VSV particles.

The addition of 19 nm gold particles promotes virus particle decoration but does not influence the virus particle distribution. However, the decoration of virions is not complete and undecorated virions can be observed by TEM as shown below.

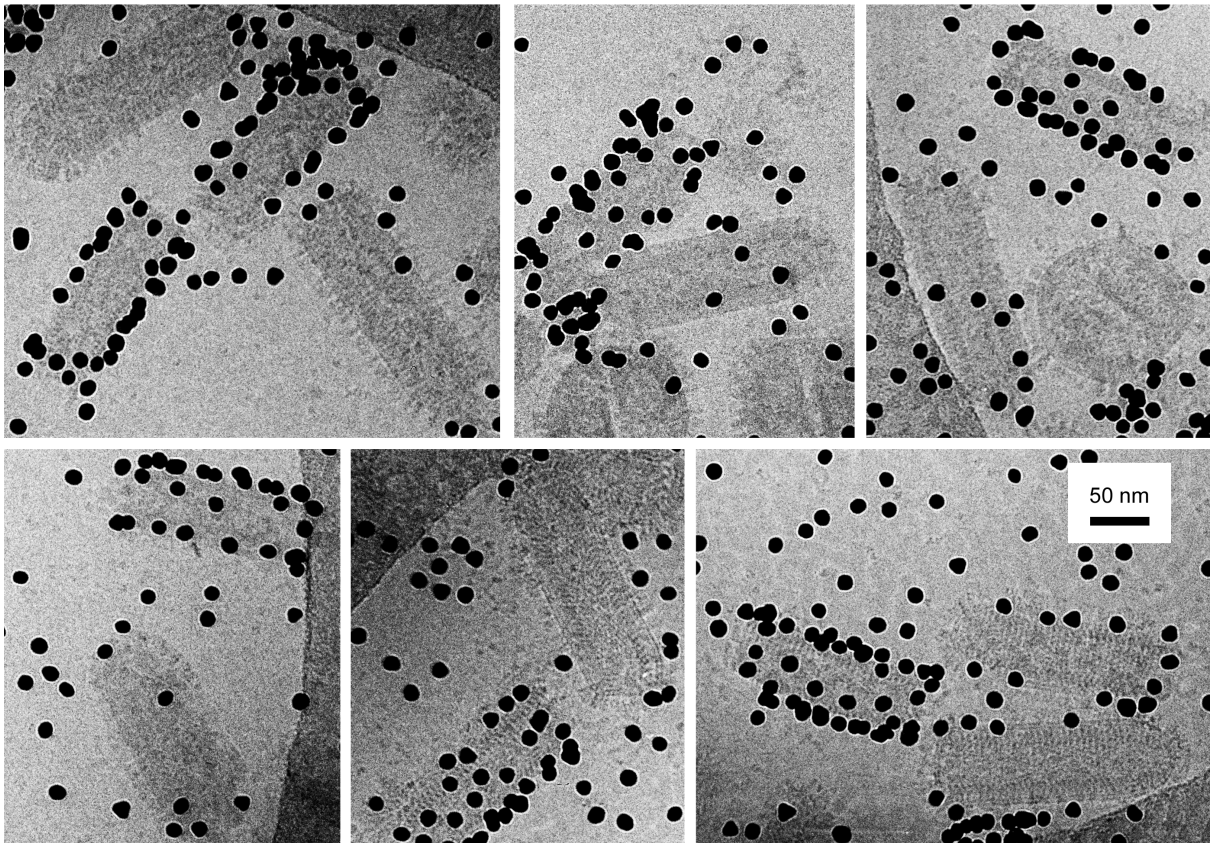

Fig. S11 Tableau of selected areas from a VSV/19 nm-AuNP preparation showing the side-by-side appearance of decorated and (nearly) undecorated virions.

As the three-dimensional arrangement of particles and virions cannot be fully unambiguously judged from two-dimensional projection images presented in Figure S11, as particles can falsely appear to be bound due to superposition effects, 3D reconstructions from a cryo-ET measurement are particularly useful to prove spatial relations.

For this we have selected a stack of slices out of a reconstructed 3D volume (Fig. S12) in order to restrict the information to a relevant volume element, where fully decorated virions can be proven to exist in the vicinity of undecorated virus particles.

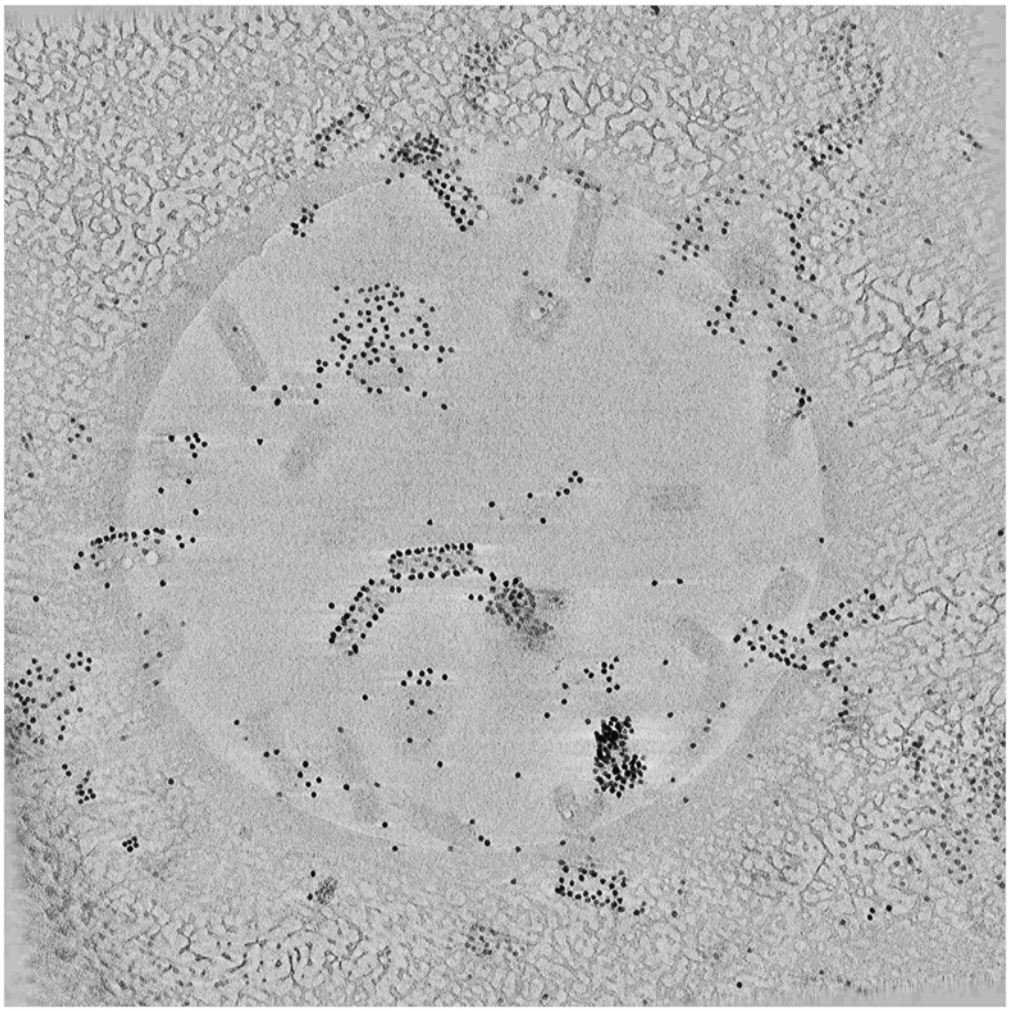

Fig. S12 Central slices of a cryo-ET reconstruction of VSV incubated with 19 nm AuNP-SO_4Na demonstrating the coexistence of fully decorated and nearly undecorated virions.

If larger gold particles (52 nm) were added, a clustering effect of virions and gold particles was observed. Due to the reasons described above, a fraction of virions is not involved in binding to gold particles and, hence, cluster formation. Within the clusters/aggregates, although virions often appear

to be spatially associated/aggregated in two-dimensional projection images (Fig. 1c), stereo images prove also in this case that virus particles not involved in cluster formation are distant and do not aggregate (see Fig. S14).

Visualization of VSV with larger sized AuNP-SO_4Na by stereoscopic cryo-TEM

After incubation of VSV and AuNP-SO_4Na for 30 min at RT a sample droplet (6 µL) was placed on hydrophilized (60 s plasma treatment at 8 W using a BALTEC MED 020 device) and perforated carbon filmed *Quantifoil* grids (R1/4 batch of Quantifoil Micro Tools GmbH, Jena, Germany). The excess fluid was blotted off to create an ultra-thin layer (typical thickness of 200-300 nm) of the solution spanning the holes of the carbon film. The grids were immediately vitrified by propelling the grid into liquid ethane at its freezing point (-184 °C). The idea of the cryo-preparation technique is to create an ultrathin amorphous glass-like sample layer by ultrafast cooling, spanning the holes of the perforated film and preserving the sample in its native state without any contact to a support layer. The vitrified samples were transferred under liquid nitrogen into a Philips Tecnai F20 transmission electron microscope (FEI company, Oregon, USA) using Gatan (Gatan Inc., California, USA) tomography cryo-holder and -stage Model CT3500. Microscopy was carried out at -175 °C sample temperature using the microscope's low dose mode at a calibrated primary magnification of 19000×. The accelerating voltage was 160 kV and the defocus was chosen to be 9.81 µm. Images at -4° and +4° specimen tilt angles were recorded using a 4k-Eagle CCD camera at 2k resolution and were subsequently aligned and combined to stereograms.

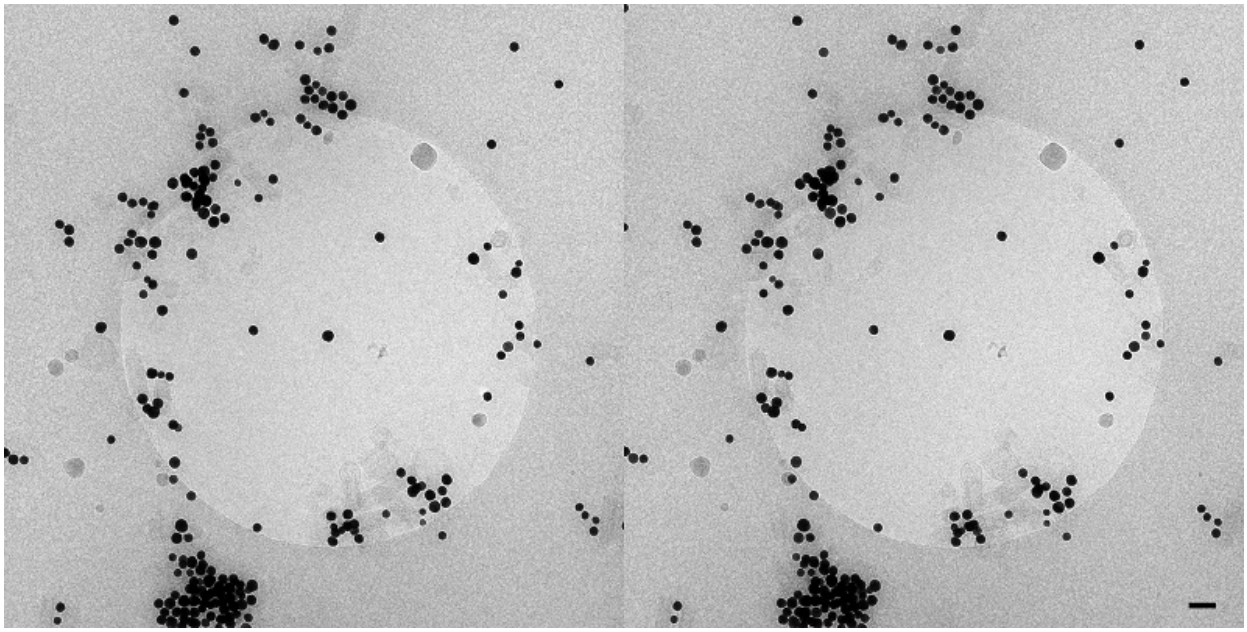

Fig. S13 VSV incubated with 39 nm AuNP-SO_4Na. Cryo-TEM stereo images (side-by-side stereogram) at an 8° view angle. Clusters of AuNP-SO_4Na and virus particles are frequently associated, although multiple binding (>1:1) of AuNP rarely occurs. Scale bar corresponds to 100 nm.

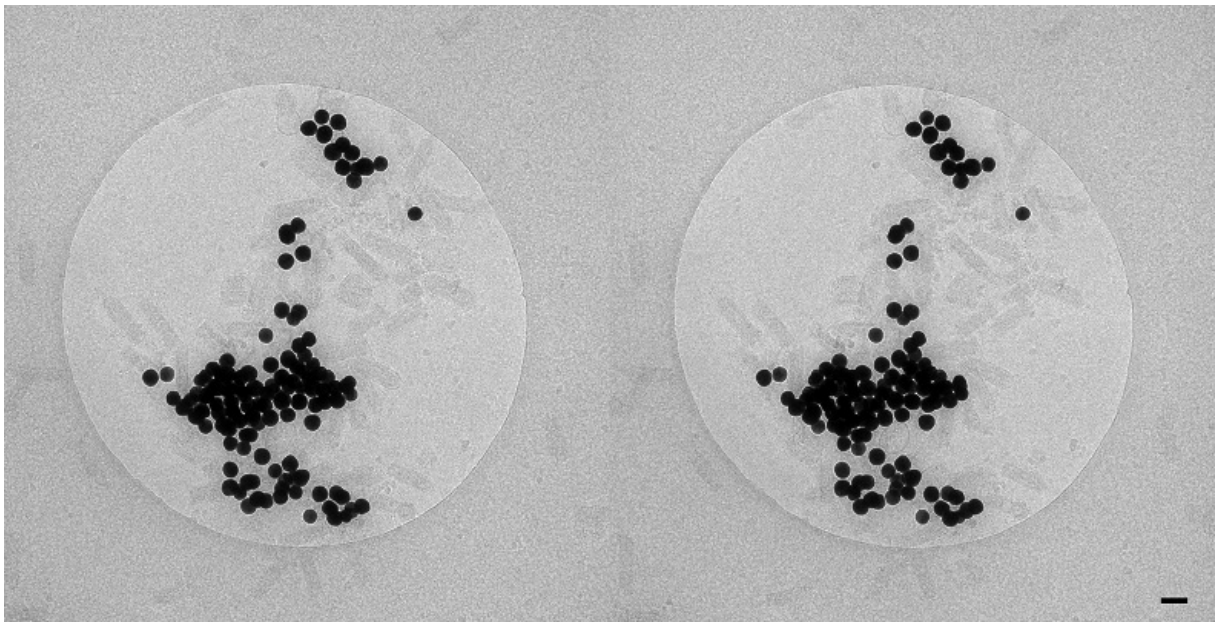

Fig S14. VSV incubated with 52 nm AuNP-SO_4Na. Cryo-TEM stereo images (side-by-side stereogram) at an 8° view angle. Clusters of AuNP-SO_4Na and virus particles, respectively are frequently associated, although multiple (>1:1) binding of Au-NP rarely occurs. Scale bar corresponds to 100 nm.

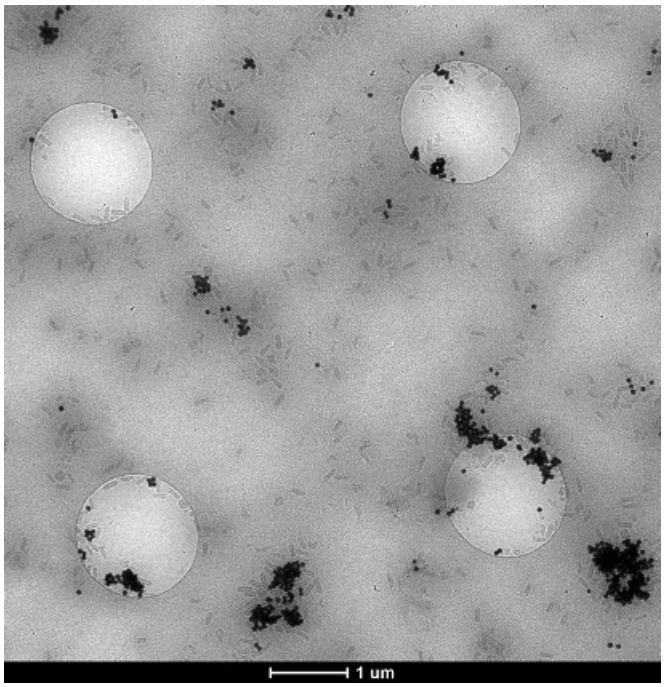

Fig. S15 Cryo-TEM overview image of VSV incubated with 52 nm AuNP-SO_4Na. The image shows a larger area (8µx8µ) of a prepared carbon film with holes covered by a vitrified sample layer. The image demonstrates the frequent formation of larger clusters of cross-linked gold and virus particles.

In order to assure no influence of the sample preparation conditions and the continuous support film on the particle distribution pattern obtained by cryo-TEM measurements, the functionalized 52 nm AuNP-SO_4Na in the absence of VSV (used concentration equal to the concentration in virus binding experiments) were recorded as in a tableau of four images presented in Figure S16.

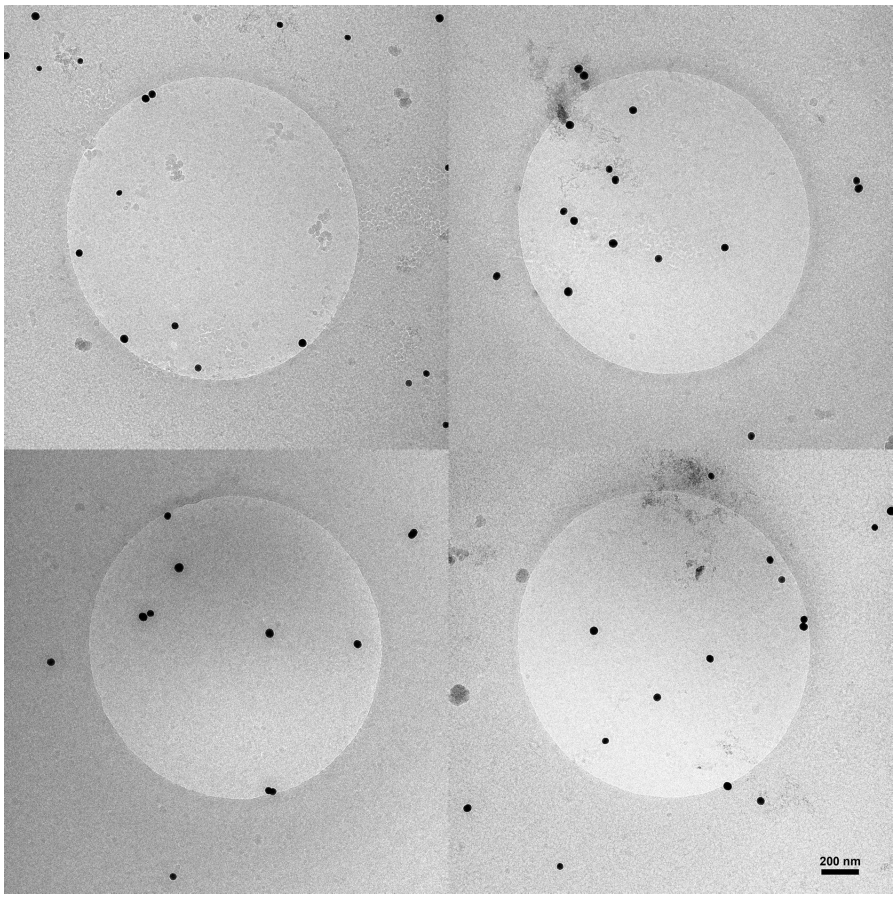

Fig. S16 Cryo-TEM images of the functionalized 52 nm AuNP-SO_4Na in absence of VSV (used with the same concentration as in virus binding experiments). Comparison with images of Figure S14 illustrates, that the aggregation effects in aqueous solution were solely caused by interaction with the VS-virions.

The cryo-TEM images of 52 nm AuNP-SO_4Na confirmed the absence of particle aggregation in the absence of VSV, which is thus exclusively induced by virus-interaction.

Estimation of the virus-particle contact area

For approximation we take the contact area between two spheres, therefore the virus was assumed to be spherical. As evident from the images in Figure 1, VSV has a rod-like shape. However, this would effect the subsequent calculations only marginally. We estimated the contact area between virus A_V and nanoparticle A_{NP} by applying a calculation based on the surface A of a spherical cap (Figure S17):

$$A = \frac{\pi\, r_{NP}\,(2hr_V - h^2)}{2(r_{NP} + r_V - h)} \qquad \text{(Eq. S5)}$$

with

$$A_V = A_{NP} = A \qquad \text{(Eq. S6)}$$

and

$$h = h_{NP} + h_V \qquad \text{(Eq. S7)}$$

We assume that the contact area between both particles is not only restricted to the contact area between two hard spheres. Because of the soft ligand shell and spike protein layer of a nanoparticle and a virus, respectively, this will also include the part of the surface, that is in a distant >=*h* between nanoparticle and virus (Figure S17). The distance between the two particles *h* is separated into a viral portion h_v and a nanoparticle portion h_{NP}. Due to the layer of spike proteins and the layer of sulfate groups on the nanoparticle, we calculate the contact area for a distance of *h*=10 nm (Figure 4). The radius of the virus was estimated from the radius of the rod shape in Figure 1a with r_v = 25 nm. Calculation of *A* in our case is based on the following equations:

$$r_V = \frac{a_V^2 + h_V^2}{2h_V} \qquad \text{(Eq. S8)}$$

$$r_{NP} = \frac{a_{NP}^2 + h_{NP}^2}{2h_{NP}} \qquad \text{(Eq. S9)}$$

With

$$a_V = a_{NP} = a \qquad \text{(Eq. S10)}$$

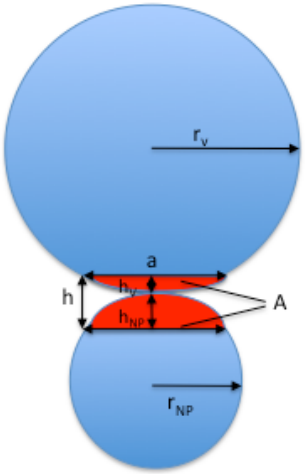

Fig. S17 Geometric model for the calculation of the virus-nanoparticle contact area.

Calculation of the relative decoration efficiency

In order to interpret the particle-calibrated virus inhibition, it is helpful to consider the number of gold nanoparticles required for a full decoration of the virion. To estimate this value, a simple calculation model was established as depicted in Figure S18.

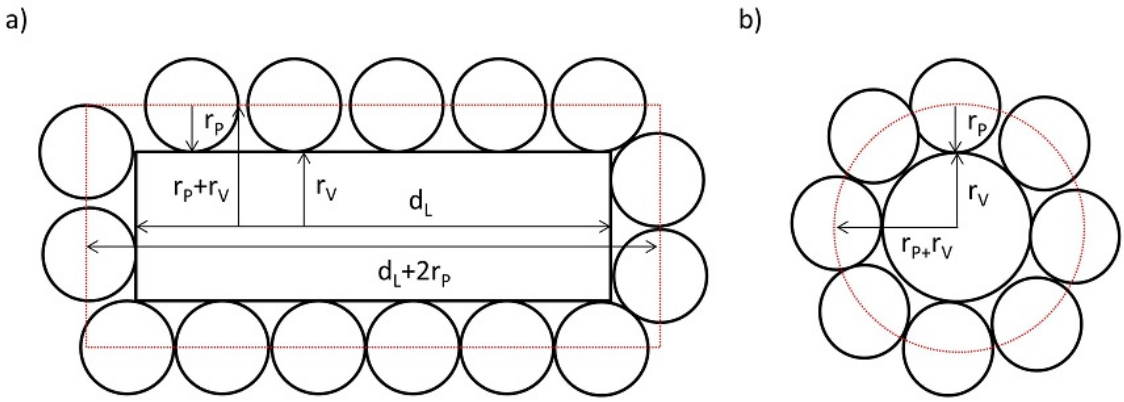

Fig. S18 Calculation model for the number of gold nanoparticles required for a full decoration of a virion. For simplification, the virion was assumed to be of cylindrical geometry. (a) side-view and (b) top-view of a nanoparticle-decorated virion.

We calculate the area of the virus A_{virus} which can be occupied by gold nanoparticles by taking the radius of the occupying nanoparticle into account as marked by the dotted, red line in Figure S16.

$$A_{virus} = 2\pi(r_V + r_P)^2 + 2\pi(r_V + r_P)(d_L + 2r_P) \qquad \text{(Eq. S11)}$$

For the calculation of the area fraction A_{hcp} occupied by gold nanoparticles, a hexagonal closed packed (hcp) arrangement was assumed as a rough estimation. The area A_V was thus multiplied with the area density factor of an hcp arrangement:

$$A_{hcp} = A_{virus}\frac{\pi}{\sqrt{12}} \qquad \text{(Eq. S12)}$$

Subsequently, the area of the cross-section of one gold nanoparticle was calculated by the following equation:

$$A_P = \pi r_P^2 \qquad \text{(Eq. S13)}$$

By dividing A_{hcp} by A_P, the number of particles per virion N_P was obtained:

$$N_P = \frac{A_{hcp}}{A_P} \qquad \text{(Eq. S14)}$$

Finally, for an estimation of the relative number of gold nanoparticles required for a full decoration of one virion in relation to the 19 nm AuNP-SO_4Na was calculated as presented in Table S3.

Table S3. Number of gold nanoparticles required for a full decoration of one individual virion and relative decoration efficiency of gold nanoparticles in relation to 19 nm AuNP.

Diameter AuNP [nm]	NP [a.u.]	Relative decoration efficiency [a.u.]
19	134	1
39	47	2.8
52	33	4
75	22	6
85	20	6.8
98	17	7.7
10	16	8.5

Concentration-dependent VSV-cell binding inhibition

In order to confirm a linear surface area dependency of the virus-cell binding inhibition, an area dependent binding-inhibition experiment was conducted for the 52 nm gold nanoparticles as depicted in Figure S19.

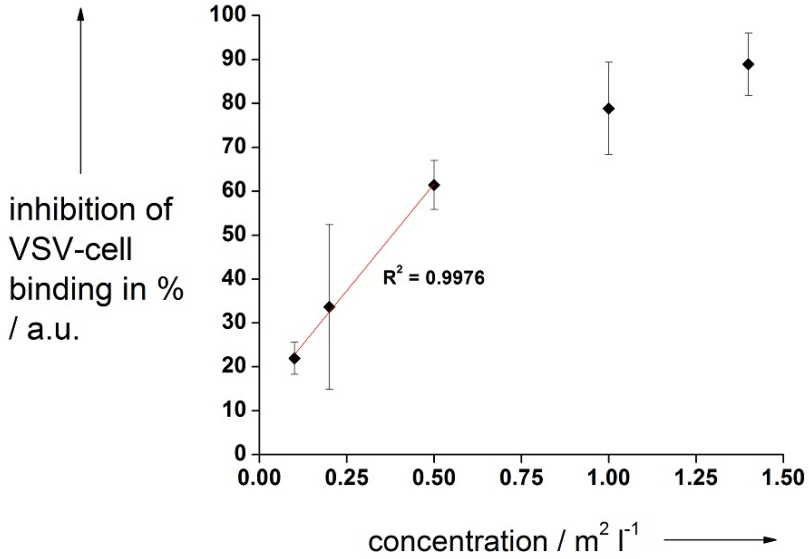

Fig. S19 Inhibition of virus-cell binding after pre-incubation with 52 nm AuNPs-SO_4Na at different concentrations. The red line confirms a linear regime for surface areas equal or below 0.5 m^2/l. Data correspond to mean +/- SEM.

The virus-cell binding inhibition plot confirms a linear relationship with respect to surface areas equal or below 0.5 m^2/l. Higher area concentrations were prone to saturation effects. A total surface area of 0.5 m^2/l was chosen as a reference due to the observed highest signal-to-noise ratio while still being in the linear regime in terms of virus-cell binding inhibition.

Cytotoxicity of the employed nanoparticles in BHK cells

To test the cytotoxicity of the used nanoparticles on BHK cells, the cell viability was measured after incubation with the indicated nanoparticles (Figure S20). BHK cells were seeded into a 96-well plate one day before the experiment. Cells were incubated with AuNP-SO_4Na (0.5 m^2/l) for 4 h at 37 °C. CellTiter-Blue reagent (Promega) was added at a ratio of 1:5 in cell culture medium and incubated for an additional hour. Fluorescence was measured on a Tecan Infinite 200 PRO plate reader.

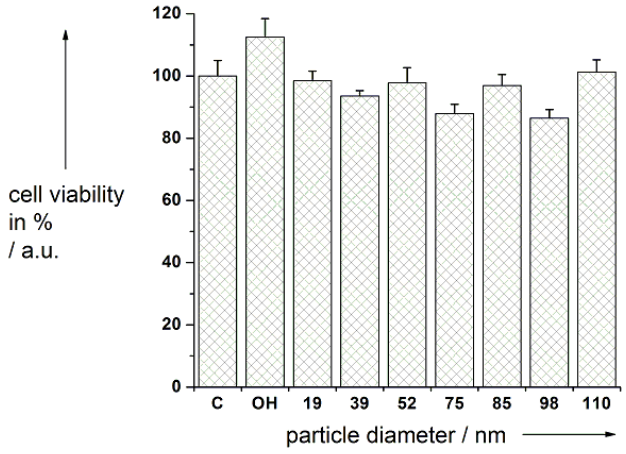

Fig. S20 Cell viability of AuNP-SO_4Na incubated BHK cells. Data correspond to mean +/- SEM.

References

1. W. Haiss, N. T. K. Thanh, J. Aveyard, and D. G. Fernig, *Anal. Chem.*, 2007, **79**, 4215–4221.

2. S. Libersou, A. a V Albertini, M. Ouldali, V. Maury, C. Maheu, H. Raux, F. de Haas, S. Roche, Y. Gaudin, and J. Lepault, *J. Cell. Biol.*, 2010, **191**, 199–210.

3. P. Arstila, *Arch. Virol*, 1976, **51**, 51–58.

4. K. a S. Thompson and J. Yin, *Virol. J.*, 2010, **7**, 257.